catalysts

MDPI

Article

Effect of B_4C/Gr on Hardness and Wear Behavior of Al2618 Based Hybrid Composites through Taguchi and Artificial Neural Network Analysis

Sharath Ballupete Nagaraju [1], Madhu Kodigarahalli Somashekara [1], Madhu Puttegowda [1,*], Hareesha Manjulaiah [1], Chandrakant R. Kini [2] and Venkatesh Channarayapattana Venkataramaiah [1]

[1] Department of Mechanical Engineering, Malnad College of Engineering (Affiliated to VTU), Hassan 573202, India
[2] Department of Aeronautical and Automobile Engineering, Manipal Institute of Technology, Manipal Academy of Higher Education, Manipal 576104, India
* Correspondence: pm@mcehassan.ac.in

Abstract: Artificial neural networks (ANNs) have recently gained popularity as useful models for grouping, clustering, and analysis in a wide range of fields. An ANN is a kind of machine learning (ML) model that has become competitive with traditional regression and statistical models in terms of useability. Lightweight composite materials have been acknowledged to be the suitable materials, and they have been widely implemented in various industrial settings due to their adaptability. In this research exploration, hybrid composite materials using Al2618 reinforced with B_4C and Gr were prepared and then evaluated for hardness and wear behavior. Reinforced alloys have a higher (approximately 36%) amount of ceramic phases than unreinforced metals. With each B_4C and Gr increase, the wear resistance continued to improve. It was found that microscopic structures and an appearance of homogenous particle distribution were observed with an electron microscope, and they revealed a B_4C and Gr mixed insulation surface formed as a mechanically mixed layer, and this served as an effective insulation surface that protected the test sample surface from the steel disc. The ANN and Taguchi results confirm that load contributed more to the wear rate of the composites.

Keywords: B_4C; Gr; Al2618; delamination wear; MMCs; ANN

Citation: Ballupete Nagaraju, S.; Kodigarahalli Somashekara, M.; Puttegowda, M.; Manjulaiah, H.; Kini, C.R.; Channarayapattana Venkataramaiah, V. Effect of B_4C/Gr on Hardness and Wear Behavior of Al2618 Based Hybrid Composites through Taguchi and Artificial Neural Network Analysis. *Catalysts* **2022**, *12*, 1654. https://doi.org/10.3390/catal12121654

Academic Editor: Leonarda Liotta

Received: 29 October 2022
Accepted: 12 December 2022
Published: 15 December 2022

1. Introduction

Aluminum was the dominant matrix in metal matrix composites due to its low density. Aluminum alloy is an elegant material with many opportunities for improvement. The beginning of the 19th century marked the beginning of numerous studies into aluminum metal matrix composites (AMMCs). Environmental and energy challenges are becoming much more significant, which is increasing the visibility of lightweight and energy-efficient products. Unfortunately, their low seizure limitation and especially their extremely poor wear resistance led to a significant reduction in their widespread use. The recent past has seen the rise of metal matrix composites (MMCs) to a considerable extent, with widespread use in a variety of air, space, and automotive/transportation equipment, as well as in electrical grids, bicycles, motorcycles, and various other products [1,2]. Many global automobile manufacturers are devoting considerable resources to replacing traditional cast iron with AMMCs in their disc brakes. Additional support was given to the base material by way of reinforcement/s, which resulted in increased structural strength. With discontinuous particulate strengthening, the possibility of production issues is greatly reduced. Strengthening the structural integrity was performed by using reinforcement/s of the base material. As discontinuous particulate strengthening is frequently utilized, production problems are typically reduced [3,4]. A significant improvement in the material's hardness is attributable to the addition of strong ceramic particles to the Al matrix. Ceramic materials have proven to be suitable for many tribological applications over the last two decades, especially in

structural areas. Al_2O_3-driven abrasive wear has the effect of depleting the composite wear resistance because of the peeling up of Al_2O_3, and it stimulates the tribo-chemical reactions that cause a decrease in wear resistance [5,6]. It is possible to see significant gains in UTS (44.35% increase) as a result of the inclusion of B_4C in Al6061.There was a rise in UTS when B_4C and SiC were added to the matrix, leading to a reduction in hardness and ductility. Lowering the coefficient of friction with incorporation in the aluminum matrix helps to encourage inclusion. In the case of higher temperatures, Gr has the ability to completely transform the chemical compositions, which influences numerous tribological characteristics. The use of the Gr is confined to the level in which its inclusion does not help to strengthen the design. The engine block was manufactured from a composite of aluminum and graphite reinforced with alumina [7–10]. Al2618 has proved useful on several spacecraft, including the Apollo missions, the Saturn V rockets, and the Space Shuttle. Aerodynamic-shaped components are easier to come by with Al2618, and the design teams appreciate this because of how well it can be welded. Al2618 was useful in aircraft and elevated temperature applications; hence, it was heavily employed in aerospace [11].

Neural networks were adopted to enhance both the accuracy and the efficiency of the slip casting process. The casting rate and humidity gradients are determined by the prediction module and configure the controllable settings for the specified environmental conditions. Based on the environment and mold and the die casting parameters, the neural network system suggests the processing time adapted to a manufacturing line [12].

The quality of the casting is determined by using an ANN. Before casting, the ANN must be trained; the casting parameters are fed into the network, after which the ideal number of hidden layers must be set. If the casting fails, it can in most situations reliably anticipate casting defects. It examines the causes of the defects and avoids the defects by changing the processing parameters of the casting. Thus, productivity can be increased [13]. An automated monitoring approach has been used to monitor the process parameters for the production of Al alloy. This method identified the defect based on X-ray defects. The ANN enables the determination of the types of defects formed during casting. Defects can be avoided by using proper casting process parameters; thus, productivity can be improved, and the cost of the casting process can also be minimized. It is observed from the result that the ANN was successfully used to achieve defect-free casting [14].

There is a scarcity of data on the effects of dry sliding wear on multi-ceramic-reinforced composites. Despite the significant difficulty in the research, it is hoped that the information gained in this study will help to define the role that hybridized composites (Al2618 + B_4C-Gr) play in a functional setting. B_4C and Gr, which are primary and secondary reinforcers, respectively, were utilized to help the Al2618 establish itself.

To determine the wear behavior of the hybridized composite more accurately, as well as that of the unreinforced Al2618, the L27 orthogonal array (Taguchi model) was used. A hardness test and a wear test were applied to the samples to learn about their hardness and wear behavior. Using SEM and XRD, the microstructure and phase analysis were evaluated. An ANN was used predict the effective parameter on the wear rate of the composites.

2. Results and Discussions

2.1. X-ray Analysis and Microstructural Study

Without the SEM, assessing the degree of damage produced by the fractures is impossible. The detection of microscopic flaws, as well as the processing problems, has been made possible through the use of microscopy. The hybrid composite is free from slag since the equiaxed grains are apparent, as illustrated in Figure 1.

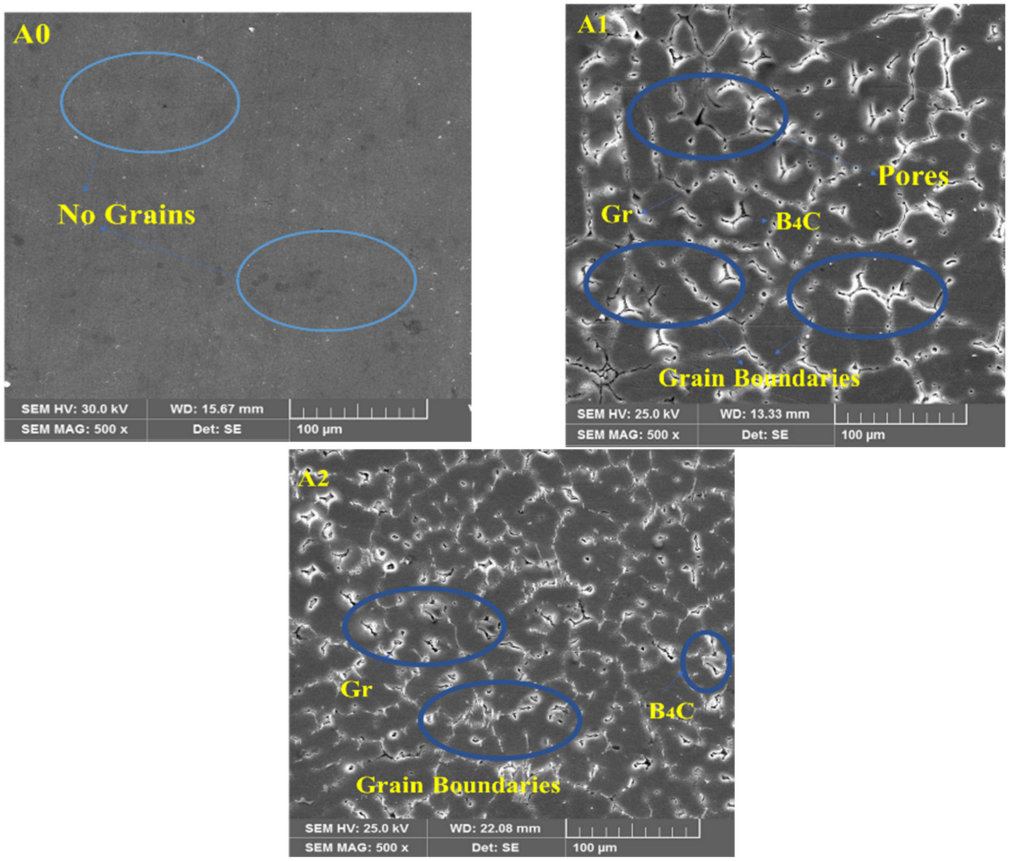

Figure 1. Microstructure of samples (A0) (Al 2618), (A1) (Al 2618 + 5% B_4C-5% Gr), and (A2) (Al 2618 + 10% B_4C-5% Gr).

The results of the XRD analysis confirm the fact that Al is present in the sample with a much greater peak. The lesser peaks found in the A1 and A2 test pins may all be attributed to the presence of B_4C and Gr. Additionally, all the test pins contain Cu, as seen in Figure 2.

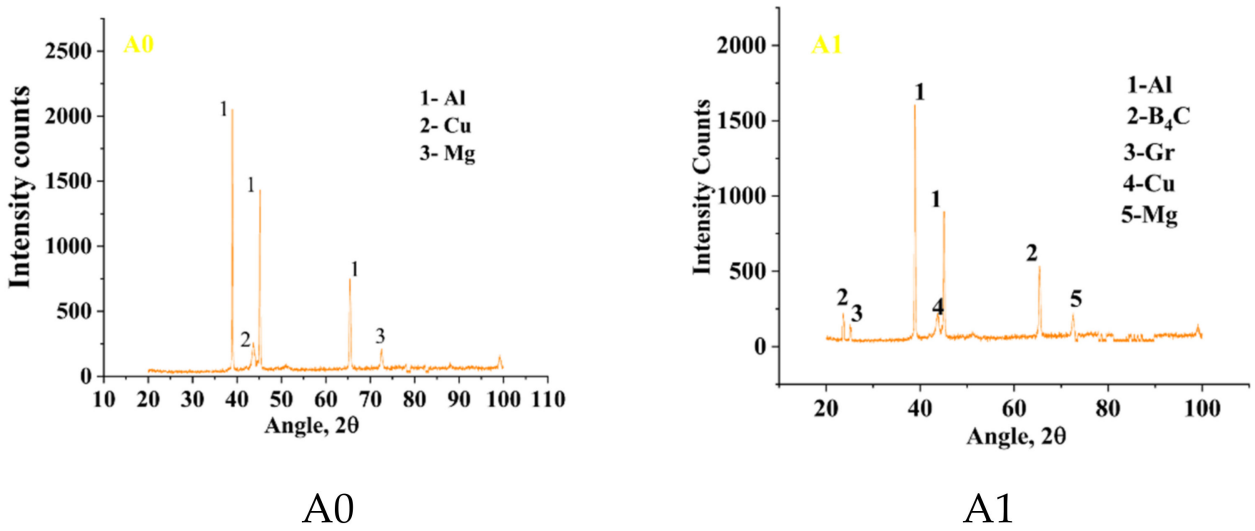

A0 A1

Figure 2. *Cont.*

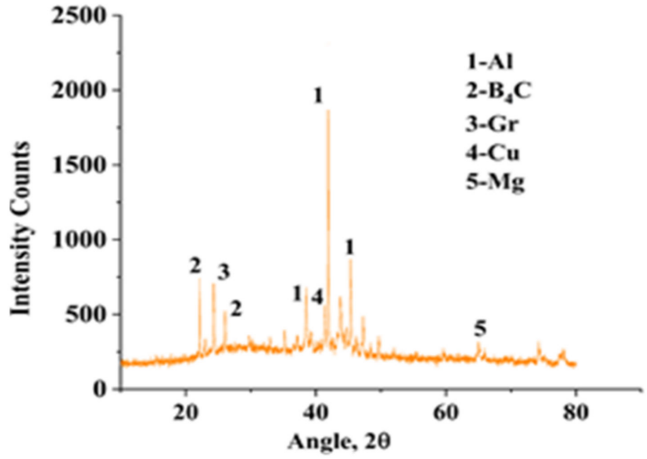

A2

Figure 2. XRD of samples (A0), (A1) and (A2).

2.2. Density and Porosity

The rule of mixing and Archimedes' principle are followed; these provide the theoretical and experimental density, respectively. Figure 3 shows the variations in density values related to the increasing weight percentage. Thus, while observing the density of the composite, the finished HMMCs were much lighter than the unreinforced Al2618 alloy. It is accepted that the density values of composites are not completely accurate as the pores and vacuums might affect the measurements. After the B_4C weight percent rose, the density value fell by around 0.13 g/cm^3. This limit of 3 to 6 percent porosity was present in the samples. Also overlooked is that the pores and other imperfections are not taken into consideration when estimating the theoretical density. This is apparent in Figure 4. Using pores in the samples causes decreased physical and mechanical characteristics. With reinforcement, the compaction of the matrix is greater, and the samples have less porosity.

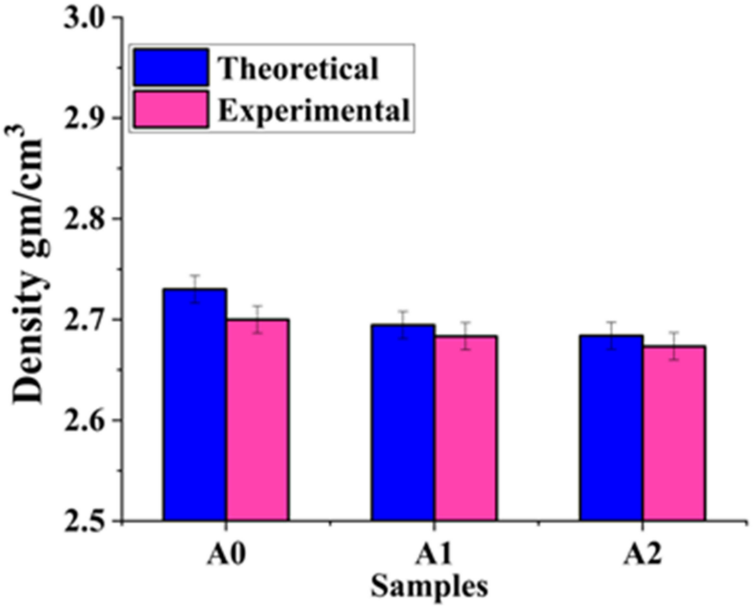

Figure 3. Theoretical and experimental density.

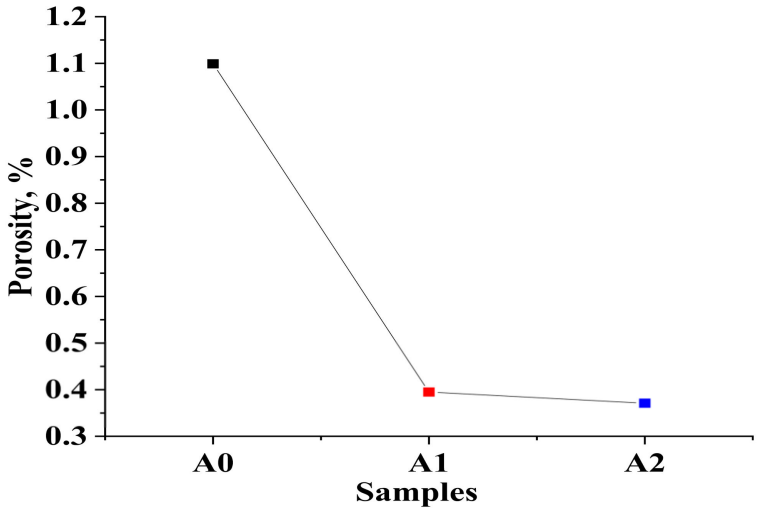

Figure 4. Porosity.

2.3. Hardness Test

This study demonstrated that the composite's hardness measures the depth of the abrasive particles that are injected into it. A softening of the composite results in less abrasion wear. According to Figure 5, as the quantity of B_4C and Gr is varied, the hardness of the resin matrix rises. With regard to the hardness values of the four test samples, the value of sample A2 is far superior (82.5 BHN). The edge of the particles in the hybridized matrix has a harder matrix due to the greater strain energy. This increases the material's resistance to penetration, which results in increased B_4C and Gr concentration in the matrix.

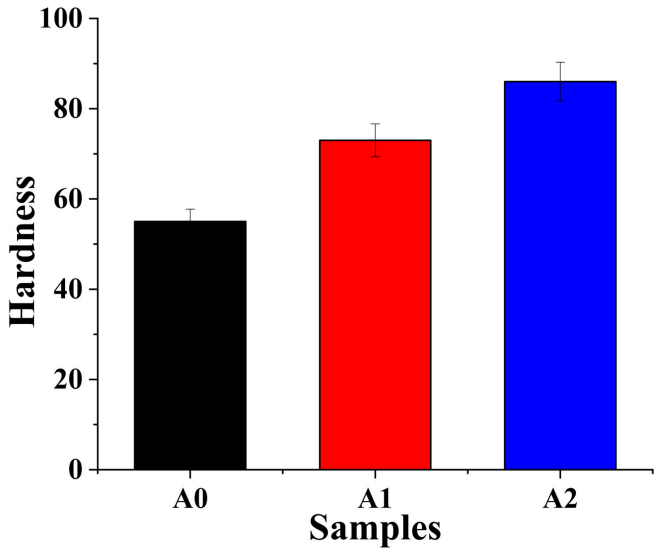

Figure 5. Hardness.

2.4. Wear Behavior

Using a pin-on-disc tribometer, the weight loss of the test samples was determined by altering the percentage of B_4C and Gr while also varying the load, speed, and distance. The experiments were conducted in accordance with the requirements set out in the Taguchi model L27. It may infer that sample A1 had a weight reduction compared to the reinforcement-free sample A0, which suggests that sample A0 lost weight while going through B_4C and Gr (A1). When hybridizing with the B_4C and Gr particles, the wear rate in the resultant matrix is less than with the non-hybridized matrix. As seen in Figure 6, due to the deposition of the thin layer on the surface of test sample A1, the wear rate decreased.

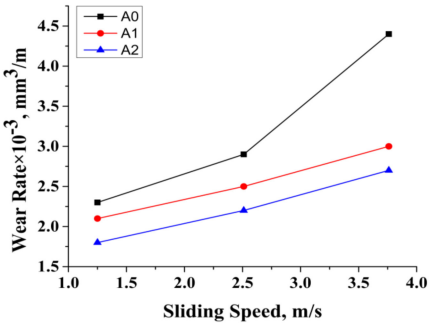

(**a**) At 20 N and 400 m.

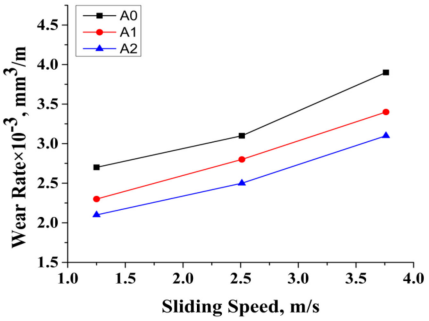

(**b**) At 20 N and 600 m.

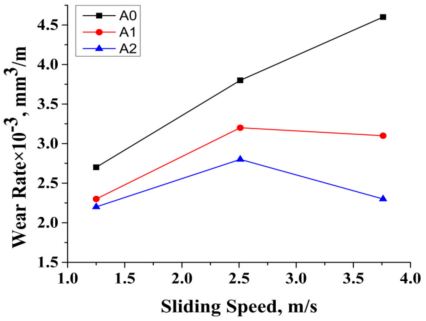

(**c**) At 20 N and 800 m.

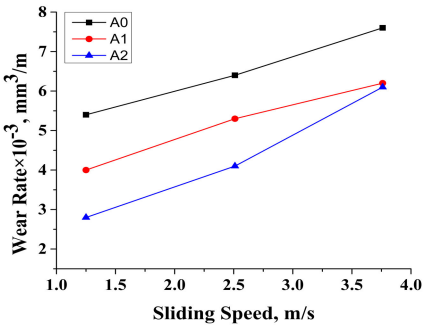

(**d**) At 30 N and 400 m.

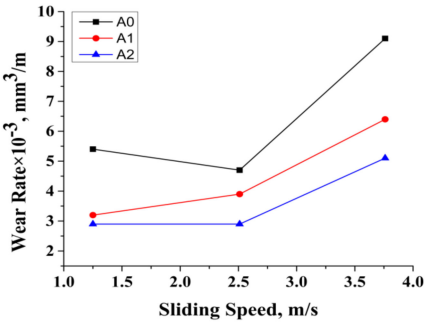

(**e**) At 30 N and 600 m

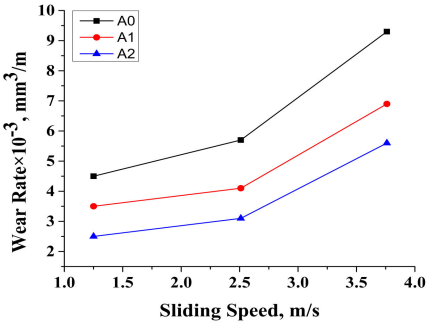

(**f**) At 30 N and 800 m

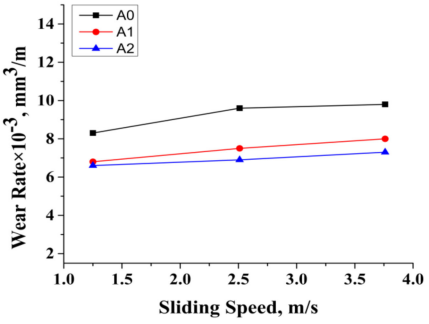

(**j**) At 40 N and 400 m.

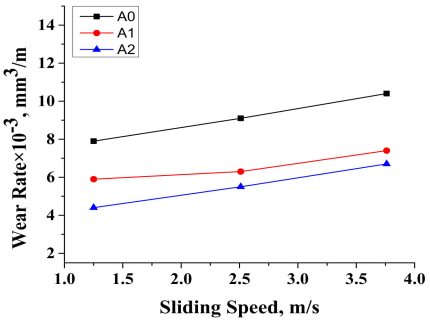

(**h**) At 40 N and 600 m.

Figure 6. *Cont.*

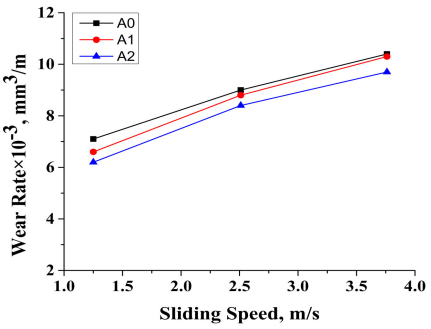

(**i**) At 40 N and 800 m.

Figure 6. Wear rate vs. speed.

Figure 6 revealed that with the increased velocity there is no appreciable movement of material from the test sample; later, it begins to increase due to the breakdown of resistive, lubricated tribo-layer. As soon as the wear starts, the strengthening particles become wear residue [15]. The wear resistance of sample A2 is higher than that of sample A0. On the other side, it displays the greater wear resistance at a lower speed, as shown in Figure 6. The splashed Gr particles from the worn composite surface form a thin and rich tribo-layer that prevents direct metallic interaction between the pin and the disc.

By reviewing Figure 6, it is evident that when the velocity is increased there is no noticeable movement of material from the test sample at the initial speed. However, the resistive tribo-layer breaks down, and the material movement increases. There is an increase in the velocity. The particles used to aid in the creation of wear are considered wear residue once wear has occurred. Sample A2 has a greater resilience to wear than sample A0. It has the lower wear resistance when it is going slower on the far side, as seen in Figure 6. The tribo-layer that results from the splashing Gr particles deposited on the worn composite surface helps to prevent direct metallic contact between the pin and the disc [16].

Sliding wear resistance improvements were not seen at a sliding distance of 400 m [17,18]. When the test sample traverses the disc, the strengthening particles have been eliminated or broken down. The mixing of materials results in the development of a mixed layer between the reinforced pin and the steel disc. The mechanical mixed layer serves to shield the test sample from wear, allowing for enhanced wear resistance. As soon as wear has been initiated on the surface of the sample, wear debris starts to appear. The various types of debris also form part of the tribo-layer; the virgin surface of the sample is therefore not in contact with the disc. While it was difficult to detect the motion, as seen in Figure 7, little movement was exhibited, and some samples were worn less as there was a high percentage of B_4C and Gr. As the test sample traveled through the disc, the strengthening particles were removed or broken down. The distribution of matter, as seen in Figure 7, is a function of the flow of material between the reinforced sample and the steel disc, which results in a mixed set of layers composed of the sample and the steel material. Using the mechanical mixed layer, the sample had the benefit of having a hard cover, which could be used to greatly enhance the resistance to wear [19].

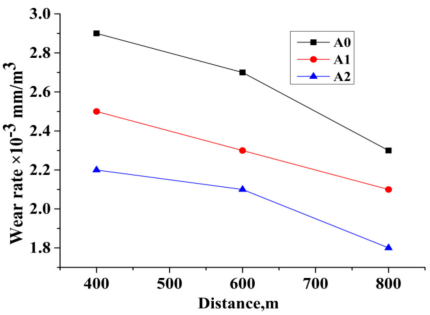

(**a**) At 20 N and 1.25 m/s.

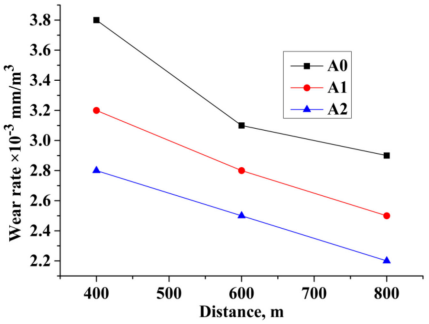

(**b**) At 20 N and 2.50 m/s.

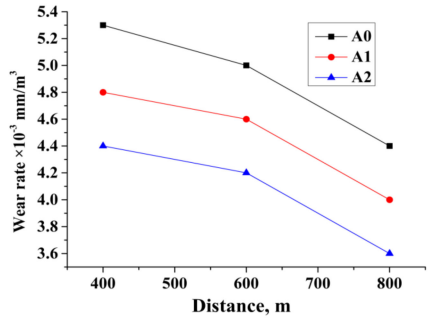

(**c**) At 20 N and 3.75 m/s.

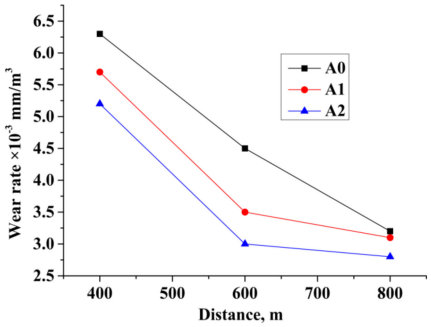

(**d**) At 30 N and 1.25 m/s.

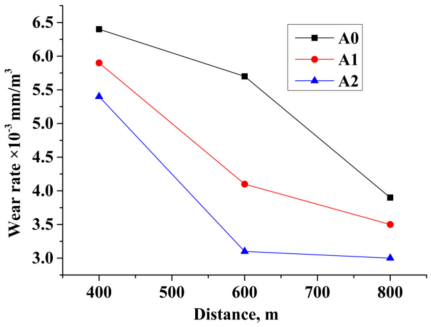

(**e**) At 30 N and 2.50 m/s.

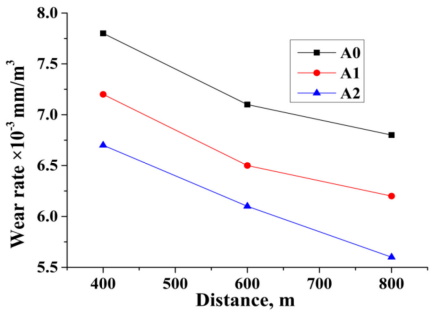

(**f**) At 30 N and 3.75 m/s.

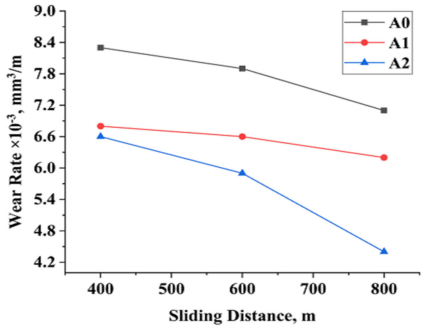

(**g**) At 40 N and 1.25 m/s.

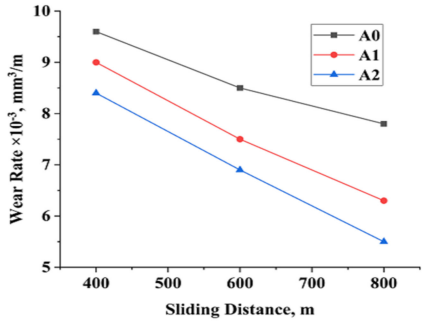

(**h**) At 40 N and 2.50 m/s.

Figure 7. *Cont.*

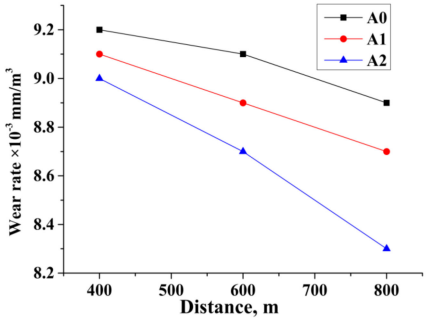

(**i**) At 40 N and 3.75 m/s

Figure 7. Wear rate vs. distance.

The increased applied load produces a rise in friction, which deteriorates the tribo-layer, and as a consequence, the wear is amplified (Figure 8). In addition to the wear rate due to the faster running, the hybrid test samples lost weight (the wear rate increased) because of the heavier load. When the distance moves higher, the A2 sample loses less weight. To lower the wear rate, the combined amount of weight and velocity must be reduced. Because of the increase in load, the tribo-layer becomes inefficient due to an increase in friction, which results in an increase in wear. Higher weights result in higher weight loss. Furthermore, the AMMC samples have a lower load-to-sliding speed that has a smaller worn surface area due to the presence of Gr particles. A B_4C and Gr-based oxide layer prevented direct metal–metal interactions, which helped to increase the wear resistance, as seen in the SEM micrographs [20].

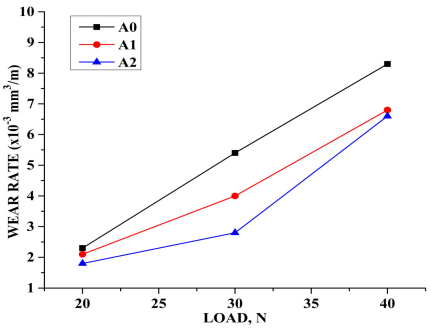

(**a**) At 400 m and 1.25 m/s.

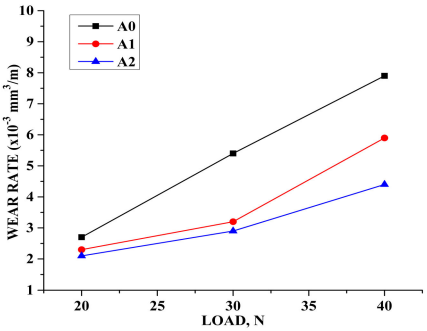

(**b**) At 600 m and 1.25 m/s.

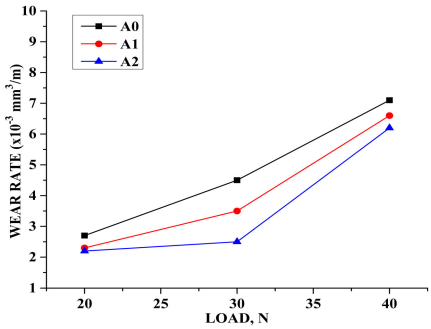

(**c**) At 800 m and 1.25 m/s.

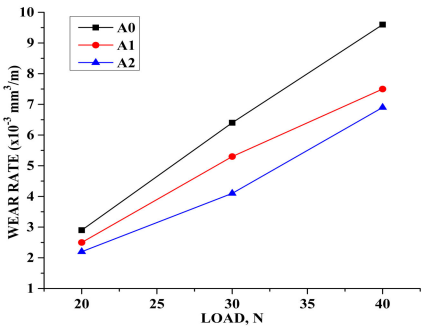

(**d**) At 400 m and 2.50 m/s.

Figure 8. *Cont.*

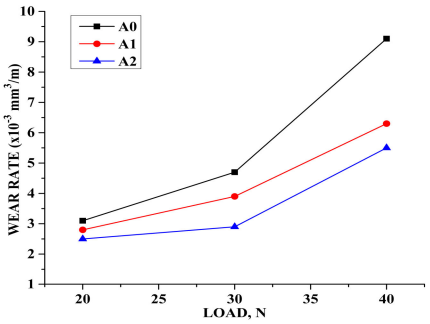

(**e**) At 600 m and 2.50 m/s.

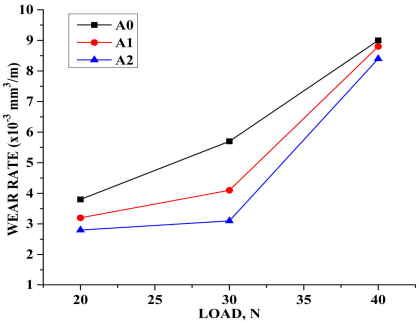

(**g**) At 800 m and 2.50 m/s.

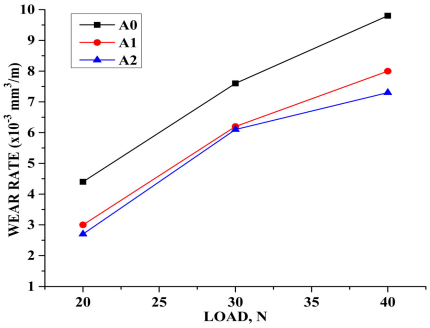

(**h**) At 400 m and 3.75 m/s.

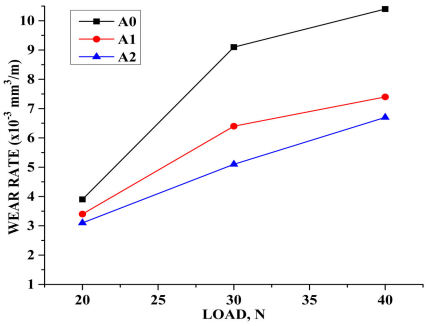

(**i**) At 400 m and 3.75 m/s.

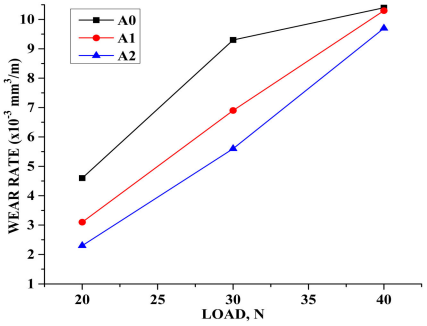

(**j**) At 400 m and 3.75 m/s.

Figure 8. Wear rate vs. load.

3. Materials and Methods

While Al2618 has not yet been found to be the most viable to build liquid cryogenic rocket fuel tanks and cylinder heads and to use in the automotive industry, it possesses exceptional features such as high strength-to-weight ratios and cryogenic characteristics, such as weldability and a near-zero coefficient of thermal expansion. As time goes on, ships are constructed of the aluminum alloy with 3 to 6 percent magnesium. This alloy offers outstanding resistance to corrosion in fresh and seawater. Therefore, the Al2618 chosen as the matrix material and its chemical composition are shown in Table 1 [11]. One of the better characteristics of B_4C ceramic is that it contains an Al matrix which causes the B_2O_3 layer to form during solidification. It belongs to the lightweight (2.52 g/cm^3) ceramic materials families, and it has an extraordinarily high neutron absorption capability. Adding B_4C to the AMMCs makes them stiffer. Additional strengthening was necessary due to this. Solid lubricants (MoS_2, Gr, and BN) are used in AMMCs, which leads to an increase in composite wear resistance. Due to the solid crystal structure, Gr has an exceptionally low friction coefficient.

Table 1. Constituents of Al2618 [11].

Element	Si	Fe	Cu	Mn	Mg	Cr	Ni	Zn	Ti	B	Ca	Al
Wt.%	0.24	1.30	2.52	0.004	1.46	0.02	1.14	0.01	0.07	0.003	0.002	Balance

In the few studies that have been conducted so far, there is considerable evidence to support the notion that switching to hybridization is effective in improving the physical properties of metal matrix composites. The present research's major goals are to advance the wear and hardness properties of the Al-Cu-Mg metal matrix composites by means of the appropriate mix and match reinforcement (Table 2) strategies; this alloy can give a higher tribological performance because of the exceptional qualities of the ceramics [21–25].

Table 2. Percentage of particulate reinforcement by weight.

Sample Designations	Composition	Al2618, %	Boron Carbide (B_4C) wt.%	Graphite (Gr) wt.%
A0	Al 2618	100	0	0
A1	Al 2618 + 5% B_4C-5% Gr	90	5	5
A2	Al 2618 + 10% B_4C-5% Gr	90	10	5

3.1. Fabrication of Composites by Using Stir Casting Method

The chemical compatibility of the matrix phase and the reinforcement is an issue for making MMCs with liquid metal casting processes such as stir casting, especially for small-scale productions. Stir casting (Figure 9) is used in the present study since it is versatile and beautiful, and it is less expensive compared to other casting techniques; these are features that appeal to researchers. Mixing reinforcement material should be conducted in a homogeneous liquid matrix phase. The Al2618 alloy billet was melted in a graphite crucible, which was set at 700 °C. Magnesium was added to the crucible to help the molten metal have better wetting qualities. A stirrer made of zirconium-coated steel was used to swirl the molten material at 160 rpm for 5–10 min. Moreover, primary reinforcement B_4C was used in conjunction with the integration of low-speed primary reinforcement. Gr was added to the premixed slurry and stirring was kept at a constant speed of 160 revolutions per minute for a period of 5 to 10 min to achieve even mixing before dumping the molten slurry into the mold cavity. Later, the manufactured part was machined to a 10 mm diameter and a 30 mm length, according to G99 standards, to conduct a wear test [26–28].

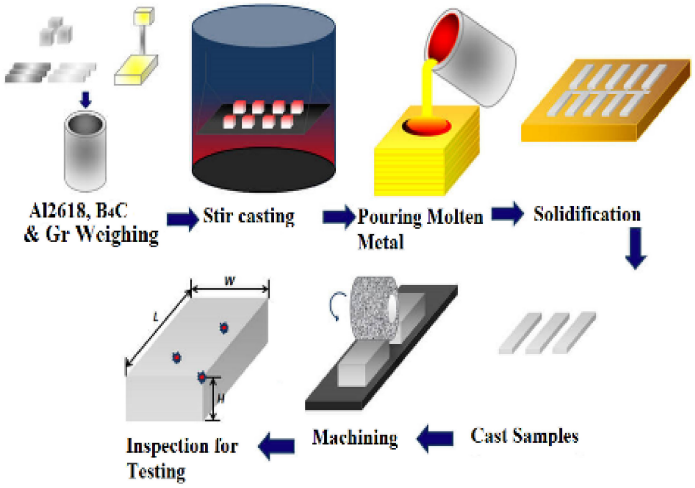

Figure 9. Stir casting steps.

3.2. X-ray Diffraction and Microstructural Study

The small defects may wreak havoc on the structural integrity of the material. SEMs have several planes that provide greater magnification and a greater depth of focus, en-

abling users to see the distribution of particles inside the material more closely. Voltages between 2 and 40 kV were used, where an electron beam of <0.01 µm in diameter was focused. An Advanced Goniometer Model 2036E201 (Bruker) with Kα radiation (Kα = 154056) was used to conduct X-ray diffraction experiments. The sample was static throughout the duration of the test, and it was scanned at a rate of 2°/min across a range of 10-80° to obtain the diffraction angle (2θ) [29].

3.3. Hardness Test

The ASTM E10 (ISO 6506: 2005) standards were used to prepare the hardness samples, accordingly. The sample hardness test was completed using a load of 250 kgf and dwell duration of 30 s [30].

3.4. Wear Test

Each of the experimental runs followed the Taguchi model (L27). The data acquisition system was attached to the disc using a friction monitor, the TR-20-PHM 400, made by DUCOM. The wear test samples were prepared according to the ASTM G99 standards. The effect of selected factors on the wear rate was investigated with the support of Minitab17, Python, and the IBM SPSS Statistics 22 framework. To move a pin against a disc (EN31 steel) was the basic working theory of the machine. A disc rotates for the given length and distance at the preset speed. Table 3 depicts the design of experiment (DOE) conditions followed in this investigation.

Table 3. Design of Experiment (DOE) Conditions.

Experimental Runs	Load (N)	Speed (m/s)	Distance (m)
1	20	1.25	400
2	20	1.25	600
3	20	1.25	800
4	20	2.51	400
5	20	2.51	600
6	20	2.51	800
7	20	3.75	400
8	20	3.75	600
9	20	3.75	800
10	30	1.25	400
11	30	1.25	600
12	30	1.25	800
13	30	2.51	400
14	30	2.51	600
15	30	2.51	800
16	30	3.75	400
17	30	3.75	600
18	30	3.75	800
19	40	1.25	400
20	40	1.25	600
21	40	1.25	800
22	40	2.51	400
23	40	2.51	600
24	40	2.51	800
25	40	3.75	400
26	40	3.75	600
27	40	3.75	800

4. Evaluation of Wear Behavior

4.1. Analysis of Factors by Taguchi Method: Mini Tab_17

Figure 10 depicts the main effect plot for the means and the residual of the experimental trials. The statistical program Minitab 17 was used to determine which factors had the

greatest impact on the wear rate. The test significance is confirmed by the residual plots for the means. The influencing elements were rated according to their degree of influence. The sliding load is the most important consideration, with speed and distance coming in last.

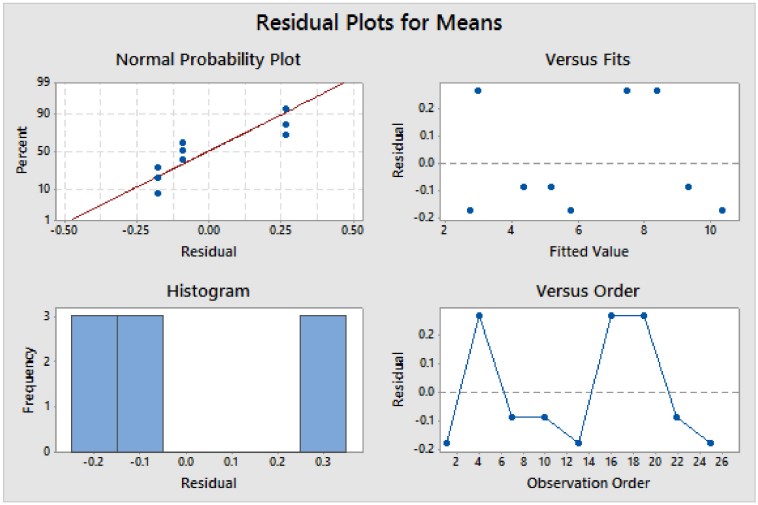

Figure 10. Residual plots for means.

The wear rate of an AMC rises with the increasing load and sliding velocity but reduces with the increasing distance [31]. The maximum wear rate figure was 1.679 mm^3/m for 40 N, 3.76 m/s, and 400 m, while the lowest was 0.419 mm^3/m for 20 N, 1.25 m/s, and 800 m. At 3.76 m/s, sliding speed had a more substantial influence on wear rate owing to the oxidative damage in this investigation. Figures 11–13 show the primary effect for the Al2618 and the reinforced Al2618 wear rates. Making decisions about the ideal testing circumstances for these control variables was made much easier due to the response graphs. It is depicted in the graphs that a transition occurred in the main effect plot when the control factor setting was changed from one stage to the next. A high main effect value was associated with the highest specific wear rate in the graphs. In Figure 11, the initial optimal condition for the test samples is 40 N, 3.76 m/s, and 800 m for the major control parameters of sliding speed and sliding distance, respectively. The wear rate rose as the amount of the applied load and the sliding speed increased, as was seen in a prior study on AMMCs [32–39].

Figure 11. Mean effect plot for sample A0.

Figure 12. Mean effect plot for sample A1.

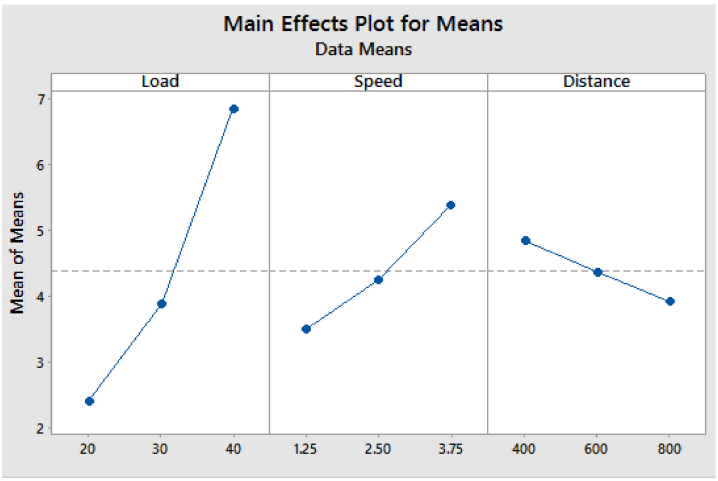

Figure 13. Mean effect plot for sample A2.

The interaction plots, as seen in Figures 11–13, illustrate the relationship between the factors and the wear rate. For each plot, one of the attributes was held constant; the impacts of the remaining two features (horizontal axis and legends) were plotted against the wear rate. For example, the first row of the first column plots sliding speed vs. wear rate at a constant distance of 400 m for various load levels, as shown in the legend. Normal load had a significant influence on wear rates, with wear rates increasing quickly as the amount of the load rose. This is a common occurrence in the vast majority of the materials studied. The size of the worn debris grew in proportion to the rise in load and friction at the pin–disc interface, which was seen to be the case. As a result, the proclivity for wear failure increases as the load is increased.

The sliding speed was the factor that had the largest influence on wear rate. When the material is exposed to sliding wear, the surface and sub-surfaces of the material deform quickly. In addition to increasing the rate of wear, the greater sliding speeds also resulted in increased heat generation and weakening of the matrix. As the sliding distance increased, the link between wear rate and sliding distance became less significant. It is possible that strain hardening is a contributing element to this phenomenon.

Figures 11–13 show the outcomes of the experiments. It is clear that the hybridized samples A1 and A2 had a reduced wear rate compared to sample A0 when the same fixed settings were used for both. It is estimated that the rate of wear for the hybridized samples is lowered by 36% for a speed of 1.25 m/s and 18% for a speed of 3.76 m/s. The increased wear resistance of the hybridized samples was discovered by examining samples that had already worn out. Afterwards, the worn-out surfaces of both the hybridized and the

unhybridized specimens were investigated using the SEM to determine the wear process and compare the severity of wear. The creation of a mechanically mixed layer and the subsequent removal of the same layer were the driving forces behind the constant/steady-state wear rate trend observed in the literature. The wear mechanism differed across samples that were and were not treated with the hybridization process. An increase in frictional resistance resulted in an increase in temperature, a softening of the matrix, and a plastic deformation, all of which contributed to a substantial increase in the wear rate. The shift from abrasive to adhesive wear was more prevalent at lower loads and more dominating at higher loading.

The Taguchi findings revealed that the sliding speed and load were the most relevant factors for the wear tests on samples A0, A1, and A2, according to the Taguchi method. The wear rate is favorably connected with both sliding speed and applied load; however, the wear rate is negatively correlated with sliding distance. In order to obtain a superior response, the load and speed must be kept at a low level, but the distance must be kept at a high level. According to these findings, ceramic reinforcements (B_4C and Gr) improve wear resistance, strength, and other tribological parameters of the components by reducing the rate of material loss and extending the service life of the components [40–48].

4.2. Analysis of Factors by Artificial Neural Network: IBMSSPSS Statistics 22

An ANN is a type of artificial intelligence modelling approach. The ANN is closely interrelated with a structure analogous to the brain cells in human neural networks and consists of a huge number of basic processing components termed neurons. The layers in the network are organized into several layers: the input layer, the output layer, and one or more hidden layers. One of the most well-known features of the ANN is its capability to learn from a sample set, referred to as the training set, throughout the learning process (multilayer perceptron method).

IBMSSPSS Statistics 22.0 was utilized to forecast the wear characteristics of the HMMCs. It requires entire experimental findings together with variables (load, speed, distance, temperature, etc.) and is supplied via the input nodes. The output nodes were utilized to produce output values and then compared to the experimental data. These activities were performed via back propagation neural networks, and the errors could be assessed. The hidden layer suggested that there was no observable connection among the neurons. All these layers were activated through the sigmoid function. Ten thousand iterations were required for accurate prediction and additional iteration cycles had no influence on the error deduction. A standardized root mean square was utilized to monitor and validate the ANN performance. Once the ANN's architecture has been specified, the wear rates were computed using a learning process in order to provide the desired output as depicted in Figure 14. The ANN assists in identifying the effect of parameters on the wear rate. The ANN helps to determine the significant wear rate-associated characteristics [19,20].

4.2.1. ANN Analysis for Sample A0

The IBM SPSS - 22 divides input vectors and target vectors into two groups by default (training = 80% and validation = 20%). The wear rate correlation factor was 0.984 between the predicted and the experimental values, utilizing the entire dataset. This is a clear sign of the proper validation by the ANN ($R2 \geq 0.90$). All points on the center axis will be the optimum forecast. The closeness of the groups on this line makes it easy to compare the accuracy of each technique. The linear fitness of a diagonal line was superior. Figure 15a indicates that various values are nearest to the centerline. The absolute relative error of the prediction technique is 0.026, which validates its accuracy. The error ranges were adequate and below the normal mistakes induced by experimental variation and measuring accuracy (Figure 15c). The important criteria for reaching greater wear rates are load (100.0%) and speed (52.8%), as described in the normalized importance (Figure 15b).

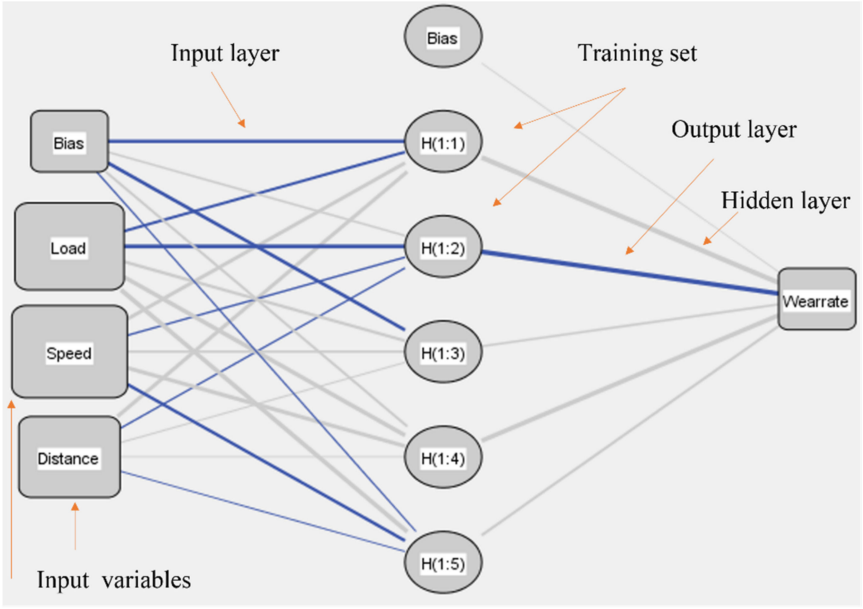

Figure 14. ANN's architecture.

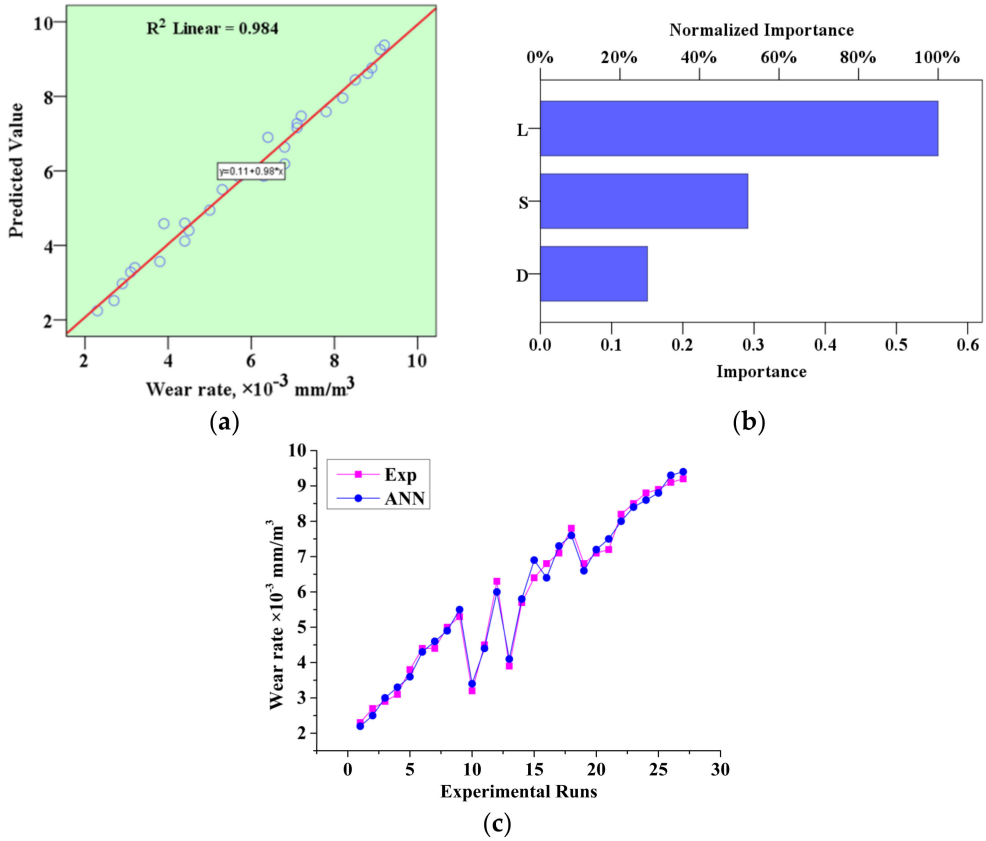

Figure 15. ANN analysis for sample A0: (**a**) experimental vs. predicted values; (**b**) normalized factor importance; and (**c**) error values.

4.2.2. ANN Analysis for Sample A1

The experimental wear rate has a relative error of around 0.031%. As a result, as indicated in Figure 16a, the variances in the anticipated values are closer to the experimental values. The normalized graph of significance (Figure 16b) indicates that the wear rate in sample A1 is increased effectively. Figure 16a shows that there are diagonally dispersed

points; this sort of dispersion is a positive indication of the higher accuracy in the ANN prediction. The findings demonstrate that the ANN predictions are very much compatible with the test values for all the input parameters (R2: 0.984). The important criteria for reaching greater wear rates are load (100%) and sliding speed (54%), as described in the normalized importance.

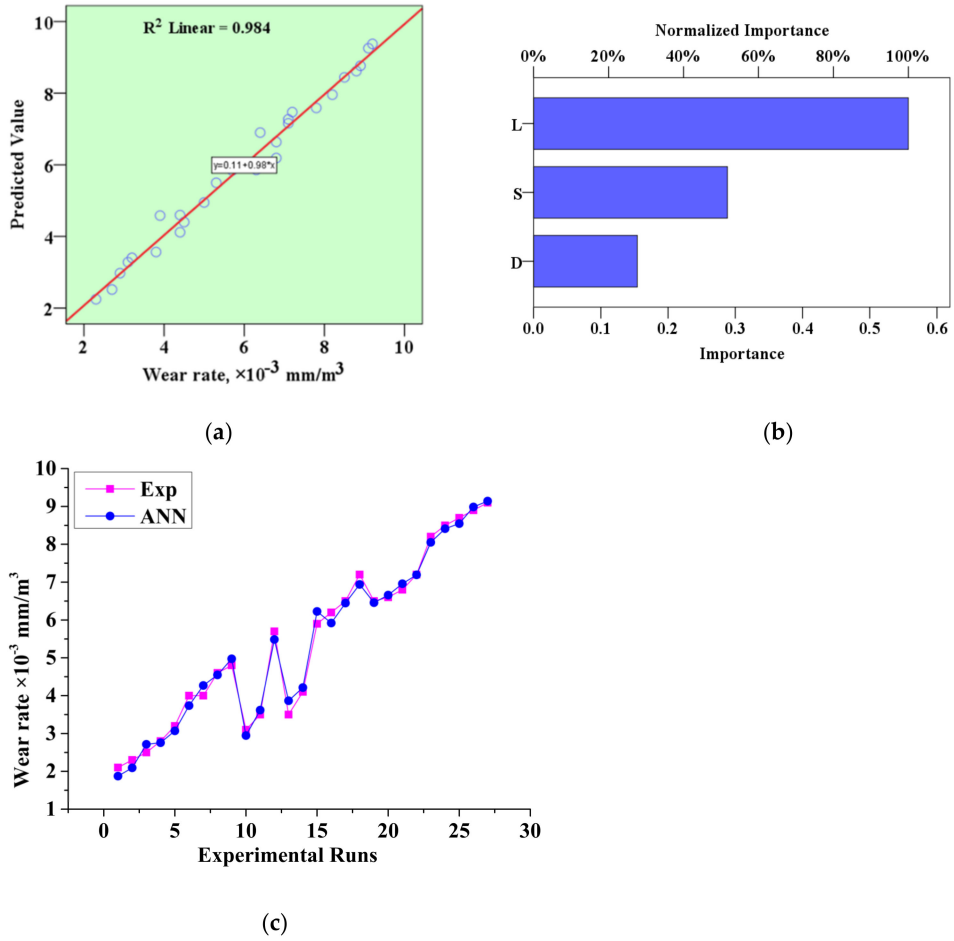

Figure 16. ANN analysis for sample A1: (**a**) experimental vs. predicted values; (**b**) normalized factor importance; and (**c**) error values.

4.2.3. ANN Analysis for Sample A2

The wear rate of sample A2 was predicted using an ANN model that took into account the influence of the operating circumstances. As a result, the predicted value fluctuations are closer to the experimental values (error = 0.064), as seen in Figure 17c. The normalized plots (Figure 17b) show that the wear rate for the sample A2 is increased by the load and speed. The findings demonstrate that the ANN predictions are well in line with the experimental values for all the input parameters (R2: 0.946). Figure 17b shows that load and speed more effectively increase the wear rate for the sample A2.

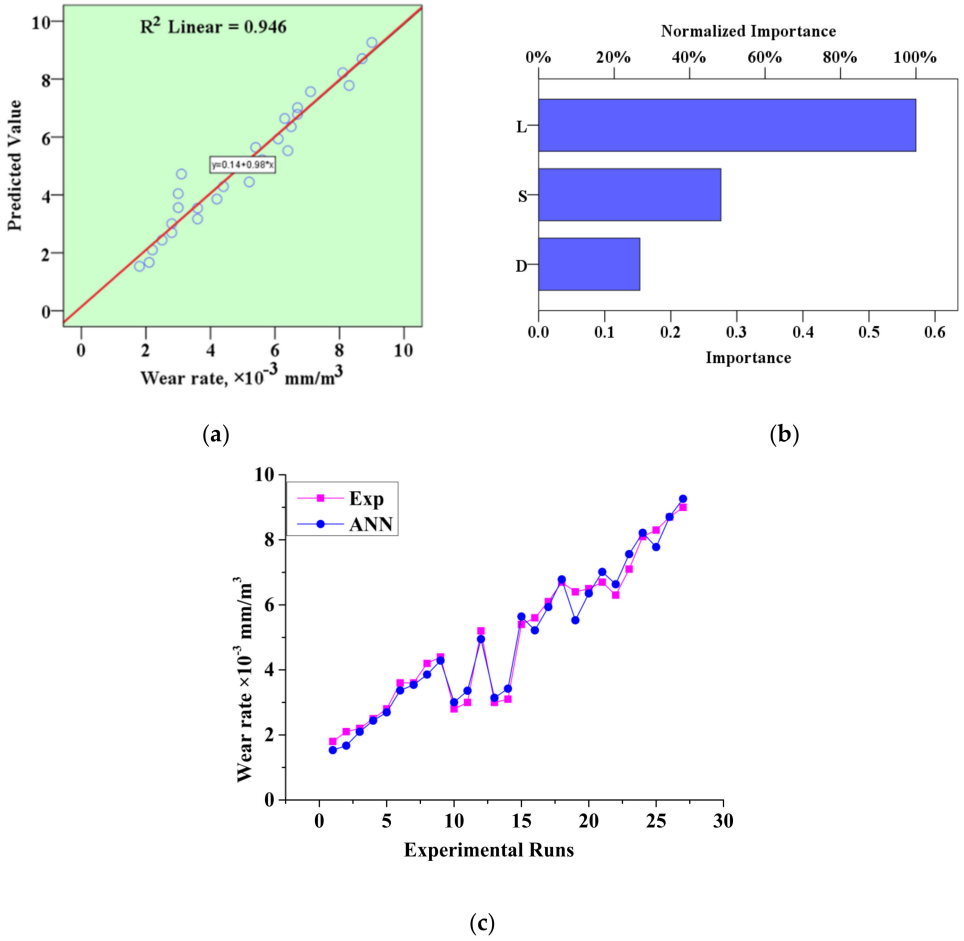

Figure 17. ANN analysis for sample A2: (**a**) experimental vs. predicted values; (**b**) normalized factor importance; and (**c**) error values.

The wear rates of samples A0, A1, and A2 were plotted using an ANN model that took into account the influence of the operating circumstances. The interaction plots help to identify the most influenceable factor to achieve a greater wear rate in the cases of both the hybridized composites and the non-hybridized composites (Figure 18). The findings demonstrate that load and speed more effectively increased the wear rates for all the samples (A0, A1, and A2).

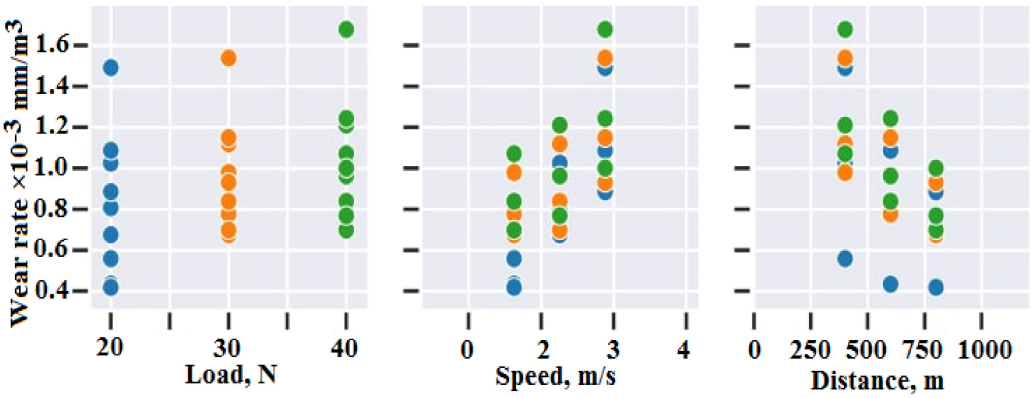

Figure 18. Interaction plot of sample A0, A1, and A2.

5. Worn Surface Morphology

These SEM micrographs show the unreinforced alloy, as well as the worn surface, which is parallel to the sliding direction. The alloy surface of sample A0 is worn, indicating that there is extensive adhesive wear, particularly with regard to the re-melt bubble and the high flow of materials. In Figure 19b,c, cuts and grooves were found among disconnected wear debris, resulting in shallower grooves running with the sliding direction. The strengthening particles are peeled from the surface, as seen in Figure 19a–c.

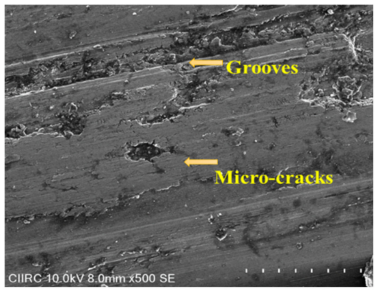

(**a**) Sample A0 At 20 N

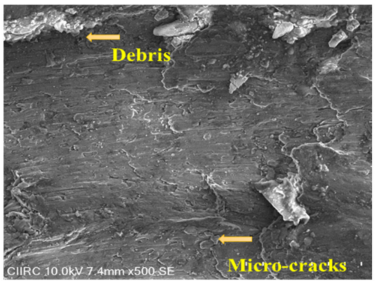

(**b**) Sample A0 At 30 N

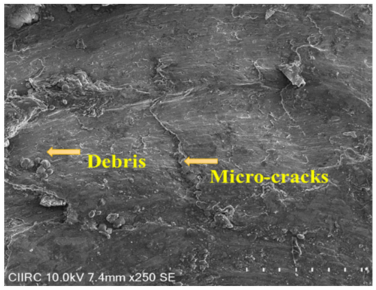

(**c**) Sample A0 At 40 N

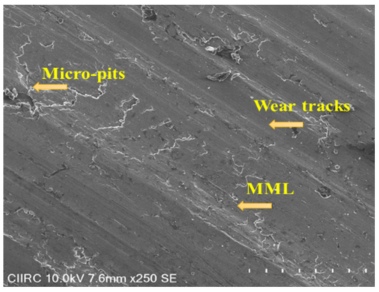

(**d**) Sample A1 At 20 N

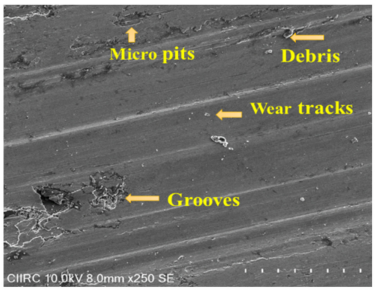

(**e**) Sample A1 At 30 N

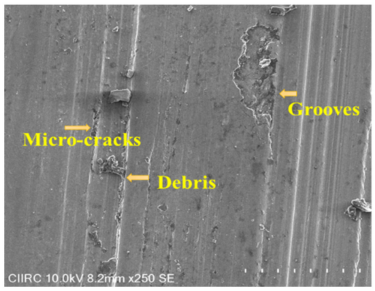

(**f**) Sample A1 At 40 N

Figure 19. *Cont*.

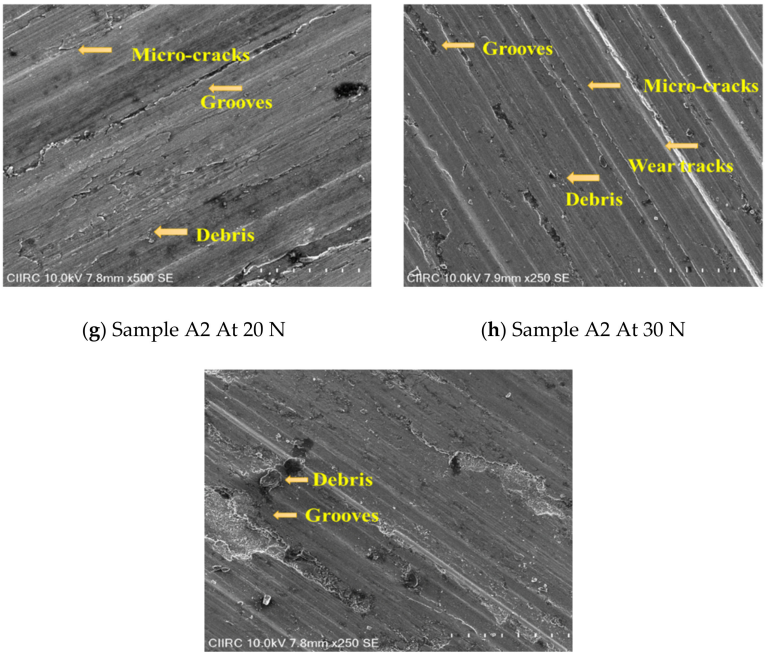

(**g**) Sample A2 At 20 N (**h**) Sample A2 At 30 N

(**i**) Sample A2 At 40 N

Figure 19. Worn surfaces of samples with respect to load (**a**–**c**)—A0; (**d**–**f**)—A1; (**g**–**i**)—A2.

Long deformation bands appear in the SEM image as well, indicating the presence of delamination wear. It can be clearly observed in Figure 19d–f that better wear resistance is the result of the deeper grooves and the reduced plastic flow, which are both seen on the A1 sample surface. In Figure 19d–i, the decreased amount of plastic flow and the more prominent grooves that appear on the sample's surface show clear evidence of better wear resistance. The weight loss is enhanced because the lubricating layer depletes and increases the depth of wear. The A1 sample reveals a rich tribological layer due to the presence of B_4C and Gr [32–35].

In the experiment, the wear rate was shown to be accompanied with a decrease in the lubricating layer, which corresponded with the theoretical conclusions. The rich tribo- layer found in the A1 sample exhibits B_4C and Gr as a direct metal-to-metal contact and avoids them altogether. For the A1 sample, the tribo-layer should be used as the defensive layer, and this was seen in weight loss reduction. The wear behavior was impacted by Al2618 and B_4C and Gr's interfacial strength. An additional resistance to abrasion can be observed in Figure 19g–i [17]. A comparison between sample A2 and A0 and A1 reveals that there is a strong tribo-layer present in sample A2, thereby resulting in reduced damage to the surface, as indicated in the SEM image.

The lower weight loss of sample A2 may be attributed to the development of a robust tribo-layer. This tribo-film keeps wear debris from penetrating, thereby protecting the surface and reducing damage. By adjusting the size and spacing of the reinforcing particles, the discs as a whole will act to facilitate the flow of material from the reinforced sample to the steel disc, resulting in layers of mechanically mixed material, as depicted in Figure 19g–i.

Using the mechanical mixed layer, the hard cover offered better protection to the test sample and resulted in improved wear resistance. Additionally, as seen in the worn surface of the A2 sample, smooth patches and minor scratches are evident. When viewed in relation to all the A0–A2 samples, the A2 sample features a deep mechanical mixed layer that helps with surface damage resistance [36–39].

6. Conclusions

The following conclusions are drawn from the present investigation:

- Hybridized composites were successfully fabricated through a liquid stir casting process.
- B_4C and Gr particles were homogenously distributed in the Al2618 matrix.
- B_4C and Gr particles were included in the B_4C and Gr particles phase, creating a barrier to dislocation and helping to increase the matrix's hardness.
- It was discovered that the degree of resistance to wear was exactly proportional to the hardness.
- The addition of the B_4C and Gr particles makes it possible to speculate that this has the effect of increasing the matrix's wear resistance.
- For the 10 wt.% B_4C and 5 wt.% Gr, the presence of a mechanically mixed layer with B_4C and Gr means the weight loss is substantially smaller.
- The ANN and Taguchi results confirm that load contributed more to the wear rate of the composites.

Author Contributions: S.B.N., M.K.S., M.P., H.M., C.R.K., V.C.V. participated in (a) conception and design or analysis and interpretation of the data; (b) drafting the article or revising it critically for important intellectual content. All authors have read and agreed to the published version of the manuscript.

Funding: This research did not receive any specific grant from funding agencies in the public, commercial, or not-for-profit sectors.

Data Availability Statement: The raw/processed data required to reproduce these findings cannot be shared at this time due to technical or time limitations.

Conflicts of Interest: The authors declare no competing interests.

References

1. Straffelini, G.; Pellizzari, M.; Molinari, A. Influence of load and temperature on the dry sliding behaviour of Al-based metal-matrix-composites against friction material. *Wear* **2004**, *256*, 754–763. [CrossRef]
2. Sharath, B.N.; Venkatesh, C.V.; Afzal, A.; Aslfattahi, N.; Aabid, A.; Baig, M.; Saleh, B. Multi ceramic particles inclusion in the aluminium matrix and wear characterization through experimental and response surface-artificial neural networks. *Materials* **2021**, *14*, 2895. [CrossRef] [PubMed]
3. Kumar, A.; Lal, S.; Kumar, S. Fabrication and characterization of A359/Al_2O_3 metal matrix composite using electromagnetic stir casting method. *J. Mater. Res. Technol.* **2013**, *2*, 250–254. [CrossRef]
4. Zhang, G.S.; Xing, J.D.; Gao, Y.M. Impact wear resistance of WC/Hadfield steel composite and its interfacial characteristics. *Wear* **2006**, *260*, 728–734. [CrossRef]
5. Uyyuru, R.K.; Surappa, M.K.; Brusethaug, S. Effect of reinforcement volume fraction and size distribution on the tribological behavior of Al-composite/brake pad tribo-couple. *Wear* **2006**, *260*, 1248–1255. [CrossRef]
6. Sharath, B.N.; Madhu, K.S.; Venkatesh, C.V. Experimental Study on Dry Sliding Wear Behaviour of Al-B_4C-Gr Metal Matrix Composite at Different Temperatures. *Appl. Mech. Mater.* **2019**, *895*, 96–101. [CrossRef]
7. Gopalakrishnan, S.; Murugan, N. Production and wear characterisation of AA 6061 matrix titanium carbide particulate reinforced composite by enhanced stir casting method. *Compos. B Eng.* **2012**, *43*, 302–308. [CrossRef]
8. Hamid, A.A.; Ghosh, P.K.; Jain, S.C.; Ray, S. Influence of particle content and porosity on the wear behaviour of cast in situ Al (Mn)–Al_2O_3 (MnO_2) composite. *Wear* **2006**, *260*, 368–378. [CrossRef]
9. Sharath, B.N.; Venkatesh, C.V. Study on Effect of boron carbide, aluminium oxide and graphite on dry sliding wear behaviour of aluminium based metal matrix composite at different temperature. *Tribol.-Finn. J. Tribol.* **2021**, *38*, 35–46.
10. Klaffke, D.; Wäsche, R.; Janakiraman, N.; Aldinger, F. Tribological characterisation of siliconcarbonitride ceramics derived from preceramic polymers. *Wear* **2006**, *260*, 711–719. [CrossRef]
11. Chikkegouda, S.P.; Gurudath, B.; Sharath, B.N.; Karthik, S.; Mahale, R.S. Mechanical and Tribological Characteristics of Aluminium 2618 Matrix Composite Reinforced with Boron Carbide. *Biointerface Res. Appl. Chem.* **2022**, *12*, 4.
12. Lam, S.S.Y.; Petri, K.L.; Smith, A.E. Prediction and optimization of a ceramic casting process using a hierarchical hybrid system of neural networks and fuzzy logic. *IISE Trans.* **2000**, *32*, 83–91. [CrossRef]
13. Karunakar, D.B.; Datta, G.L. Prevention of defects in castings using back propagation neural networks. *Int. J. Adv. Manuf. Technol.* **2007**, *39*, 1111–1124. [CrossRef]
14. Dobrzanski, L.A.; Krupiński, M.; Zarychta, P.; Maniara, R. Analysis of influence of chemical composition of Al-Si-Cu casting alloy on formation of casting defects. *J. Achiev. Mater. Manuf. Eng.* **2007**, *21*, 53–56.
15. Baradeswaran, A.; Perumal, A.E. Study on mechanical and wear properties of Al 7075/Al_2O_3/graphite hybrid composites. *Compos. B Eng.* **2014**, *56*, 464–471. [CrossRef]

16. Hu, Q.; McColl, I.R.; Harris, S.J.; Waterhouse, R.B. The role of debris in the fretting wear of a SiC reinforced aluminium alloy matrix composite. *Wear* **2000**, *245*, 10–21. [CrossRef]
17. Ayvaz, S.I.; Arslan, D.; Ayvaz, M. Investigation of mechanical and tribological behavior of SiC and B_4C reinforced Al-Zn-Mg-Si-Cu alloy matrix surface composites fabricated via friction stir processing. *Mater. Today Commun.* **2022**, *31*, 103419. [CrossRef]
18. Senthilkumar, N.; Tamizharasan, T.; Anbarasan, M. Mechanical characterization and tribological behaviour of Al-Gr-B_4C metal matrix composite prepared by stir casting technique. *Int. J. Adv. Eng.* **2014**, *1*, 48–59.
19. LLorca, J. High temperature fatigue of discontinuously-reinforced metal–matrix composites. *Int. J. Fatigue* **2002**, *24*, 233–240. [CrossRef]
20. Rao, P.S.; Sivadasan, K.G.; Balasubramanian, P.K. Structure-property correlation on AA 2219 aluminium alloy weldments. *Bull. Mater. Sci.* **1996**, *19*, 549–557.
21. Auradi, V.; Rajesh, G.L.; Kori, S.A. Processing of B_4C Particulate Reinforced 6061Aluminum Matrix Composites by Melt Stirring Involving Two-step Addition. *Procedia Manuf.* **2014**, *6*, 1068–1076.
22. Cho, M.H.; Ju, J.; Kim, S.J.; Jang, H. Tribological properties of solid lubricants (graphite, Sb_2S_3, MoS_2) for automotive brake friction materials. *Wear* **2006**, *260*, 855–860. [CrossRef]
23. Suresha, S.; Sridhara, B.K. Effect of silicon carbide particulates on wear resistance of graphitic aluminium matrix composites. *Mater. Des.* **2010**, *31*, 4470–4477. [CrossRef]
24. Khan, A.; Puttegowda, M.; Jagadeesh, P.; Marwani, H.M.; Asiri, A.M.; Manikandan, A.; Khan, A.A.P.; Ashraf, G.M.; Rangappa, S.M.; Siengchin, S. Review on Nitride compounds and its polymer composites: A multifunctional material. *J. Mater. Res. Technol.* **2022**, *18*, 2175–2193. [CrossRef]
25. Krakhmalev, P.V.; Bergström, J. Tribological behavior and wear mechanisms of $MoSi_2$-base composites sliding against AA6063 alloy at elevated temperature. *Wear* **2006**, *260*, 450–457. [CrossRef]
26. Kala, H.; Mer, K.K.S.; Kumar, S.A. Review on Mechanical and Tribological Behaviors of Stir Cast Aluminum Matrix Composites. *Procedia Mater. Sci.* **2014**, *6*, 1951–1960. [CrossRef]
27. Patil, M.B.; Rajamani, S.B.; Mathad, S.N.; Patil, A.Y.; Hussain, M.A.; Alorfii, H.S.; Khan, A.; Asiri, A.M.; Khan, I.; Puttegowda, M. Microwave-assisted synthesis of poly (acrylamide-co-2-hydroxyethyl methacrylate)/chitosan semi-IPN ZnO nanocomposite membranes for food packaging applications. *J. Mater. Res. Technol.* **2022**, *20*, 3537–3548. [CrossRef]
28. Khanna, V.; Kumar, V.; Bansal, S.A. Mechanical properties of aluminium-graphene/carbon nanotubes (CNTs) metal matrix composites: Advancement, opportunities and perspective. *Mater. Res. Bull.* **2021**, *138*, 111224. [CrossRef]
29. Jayaprakash, D.; Niranjan, K.; Vinod, B. Studies on Mechanical and Microstructural Properties of Aluminium Hybrid Composites: Influence of SiC/Gr Particles by Double Stir-Casting Approach. *Silicon* **2022**, 1–15. [CrossRef]
30. Dey, A.; Khan, M.M. MCD approach for assessing the optimal operating condition during sliding wear characteristics of LM25/SiC AMCs processed by an improved stir casting technique. *Silicon* **2022**, *14*, 3673–3691. [CrossRef]
31. NG, S.K.; Ravindranath, V.M.; GS, S.S. Dry sliding wear behavior of hybrid metal matrix composites. *Int. J. Res. Eng. Technol.* **2014**, *3*, 554–558.
32. Hayajneh, M.T.; Hassan, A.M.; Mayyas, A.T. Artificial neural network modeling of the drilling process of self-lubricated aluminum/alumina/graphite hybrid composites synthesized by powder metallurgy technique. *J. Alloy. Compd.* **2009**, *478*, 559–565. [CrossRef]
33. Alam, M.T.; Ansari, A.H. X-ray diffraction analysis and microstructural examination of al-sic composite fabricated by stir casting. *Int. J. Sci. Technol. Manag.* **2015**, *4*, 941–956.
34. Suresha, S.; Sridhara, B.K. Friction characteristics of aluminium silicon carbide graphite hybrid composites. *Mater. Des.* **2012**, *34*, 576–583. [CrossRef]
35. Basavarajappa, S.; Chandramohan, G.; Davim, J.P. Application of Taguchi techniques to study dry sliding wear behaviour of metal matrix composites. *Mater. Des.* **2007**, *28*, 1393–1398. [CrossRef]
36. Prasad, D.S.; Shoba, C. Hybrid composites—A better choice for high wear resistant materials. *J. Mater. Res. Technol.* **2014**, *3*, 172–178. [CrossRef]
37. Mahdavi, S.; Akhlaghi, F. Effect of the graphite content on the tribological behavior of Al/Gr and Al/30SiC/Gr composites processed by in situ powder metallurgy (IPM) method. *Tribol. Lett.* **2011**, *44*, 1–12. [CrossRef]
38. Alaneme, K.K.; Sanusi, K.O. Microstructural characteristics, mechanical and wear behaviour of aluminium matrix hybrid composites reinforced with alumina, rice husk ash and graphite. *Eng. Sci. Technol. Int. J.* **2015**, *18*, 416–422. [CrossRef]
39. Baradeswaran, A.E.P.A.; Perumal, A.E. Influence of B_4C on the Tribological and Mechanical Properties of Al 7075-B_4C Composites. *Compos. B Eng.* **2013**, *54*, 146–152. [CrossRef]
40. Şenel, M.C.; Kanca, Y.; Gürbüz, M. Reciprocating sliding wear properties of sintered Al-B_4C composites. *J. Miner. Metall.* **2022**, *29*, 1261–1269. [CrossRef]
41. Halil, K.; İsmail, O.; Sibel, D.; Ramazan, Ç. Wear and mechanical properties of Al6061/SiC/B_4C hybrid composites produced with powder metallurgy. *J. Mater. Res. Technol.* **2019**, *8*, 5348–5361. [CrossRef]
42. Alizadeh, A.; Abdollahi, A.; Biukani, H. Creep behavior and wear resistance of Al 5083 based hybrid composites reinforced with carbon nanotubes (CNTs) and boron carbide (B_4C). *J. Alloy. Compd.* **2015**, *650*, 783–793. [CrossRef]
43. Radhika, N.; Sasikumar, J.; Sylesh, J.L.; Kishore, R. Dry reciprocating wear and frictional behaviour of B_4C reinforced functionally graded and homogenous aluminium matrix composites. *J. Mater. Res. Technol.* **2020**, *9*, 1578–1592. [CrossRef]

44. Madhu, K.S.; Venkatesh, C.V.; Sharath, B.N.; Karthik, S. Characterization and Evaluation of Mechanical Properties of Al-Zn Based Hybrid Metal Matrix Composites. *Appl. Sci. Eng. Prog.* **2022**, *16*, 5804. [CrossRef]
45. Şenel, M.C.; Üstün, M. Dry Sliding Wear and Friction Behavior of Graphene/ZrO_2 Binary Nanoparticles Reinforced Aluminum Hybrid Composites. *Arab. J. Sci. Eng.* **2022**, *24*, 9253–9269. [CrossRef]
46. Özbek, N.A.; Karadag, M.İ.; Özbek, O. Optimization of flank wear and surface roughness during turning of AISI 304 stainless steel using the Taguchi method. *Mater. Test.* **2020**, *62*, 957–961. [CrossRef]
47. Vedrtnam, A.; Kumar, A. Fabrication and wear characterization of silicon carbide and copper reinforced aluminium matrix composite. *Mater. Discov.* **2017**, *9*, 16–22. [CrossRef]
48. Özbek, N.A. Optimization of flank wear and surface quality in the turning of 1.2343 tool steel using carbide tools coated via different methods. *Surf. Topogr. Metrol. Prop.* **2021**, *9*, 025028. [CrossRef]